https://doi.org/10.5194/essd-2026-922
Preprint. Discussion started: 19 November 2026
© Author(s) 2026. CC BY 4.0 License.



Open Access Earth System Science Data Discussions

Twenty Years of data from the RAPID-MOCHA-WBTS array: Long-Term Changes in the Atlantic Meridional Overturning Circulation, Heat and Freshwater Transports

Tillys Petit[1], Shane Elipot[2], David A. Smeed[1], William E. Johns[2], Ryan H. Smith[3], Denis L. Volkov[4], Brian A. King[1], Elaine L. McDonagh[1], Darren Rayner[1], Julie Collins[1], Adam Ward[1] and Ben I. Moat[1]

[1]National Oceanography Centre, Southampton, UK
[2]Rosenstiel School of Marine, Atmospheric, and Earth Science, University of Miami, Coral Gables, FL, USA
[3]Atlantic Oceanographic and Meteorological Laboratory, NOAA, Miami, FL, USA
[4]Cooperative Institute for Marine and Atmospheric Studies, University of Miami, Miami, FL, USA

Correspondence to: Tillys Petit (Tillys.Petit@noc.ac.uk)

Abstract. The RAPID-MOCHA-WBTS (RAPID) array, an international collaboration between the National Oceanography Centre, the University of Miami, and NOAA, has provided more than two decades of continuous observations near 26°N, establishing an unprecedented record of the North Atlantic ocean circulation. These sustained measurements are essential for understanding how variations in ocean circulation influence regional and global climate patterns. Since April 2004, the array has provided continuous estimates of the Atlantic Meridional Overturning Circulation (AMOC) in both depth and density coordinates, as well as meridional heat and freshwater transports and other key measurements of the North Atlantic ocean circulation. As the observational record now exceeds 20 years, its length enables the investigation of robust long-term changes. Here, we present the RAPID data products, how the timeseries are derived and distributed, and present their mean, standard deviation and linear trends. We also introduce the RAPID code used to generate these data products in an effort to support reproducibility and future applications of the dataset.

1 Introduction

The Atlantic Meridional Overturning Circulation (AMOC) is a central component of the climate system. Characterized by northward transport of warm surface water and a compensating southward transport of cold deep water, it redistributes heat, carbon, freshwater and nutrient around the Atlantic (Srokosz et al., 2012). Understanding how the AMOC is changing is thus essential for assessing ocean circulation change and whether the projected weakening of the circulation under rising greenhouse gases is already under way (IPCC, 2021). Before 2004, estimates of the AMOC strength and associated heat transport came from transatlantic hydrographic sections (Bryden & Hall, 1980; Roemmich & Wunsch, 1985). These snapshots gave valuable information on the AMOC magnitude, but they could not resolve its variability (Cunningham et al., 2007). The RAPID-MOCHA-WBTS (RAPID-Meridional Overturning Circulation and Heatflux Array-Western Boundary Time Series, henceforth

https://doi.org/10.5194/essd-2026-922
Preprint. Discussion started: 19 November 2026
© Author(s) 2026. CC BY 4.0 License.



RAPID) array was designed to fill this gap by providing a continuous, accurate record of the AMOC and of the associated heat and freshwater transports.

The RAPID array spans the subtropical North Atlantic from the Florida Straits to the continental slope off Africa at 26°N, close to the latitude where the oceanic meridional heat transport is at its maximum (Trenberth & Caron, 2001). The array is operated since April 2004 by an international collaboration of three groups: the UK National Oceanography Centre, funded by the Natural Environment Research Council, the University of Miami, funded by the US National Science Foundation, and the US National Oceanic and Atmospheric Administration's Atlantic Oceanographic and Meteorological Laboratory (NOAA AOML). Together, these groups combine measurements of the Florida Current and of the flow on the Bahamian continental slope, and geostrophic transport estimates from moorings deployed along each boundary, which are all required to estimate the AMOC at 26°N.

Over the last two decades, the RAPID array has transformed our understanding of the AMOC and provided critical evidence of ocean variability and change. For example, it has revealed substantial AMOC variability on timescales ranging from days to decades (Kanzow et al., 2010; McCarthy et al., 2012; Smeed et al., 2014). The record also provides the observational benchmarks needed for evaluating ocean models, reanalyses, and climate models, thereby helping to improve our confidence in future projections of climate and ocean change (Jackson et al., 2016; Winkelbauer et al., 2026; Yan et al., 2018). The RAPID array has also evolved over time. Combined with repeated hydrographic sections and Argo profiles in the basin interior, it has enabled estimates of the meridional heat transport (Johns et al., 2011, 2023) and freshwater transport (McDonagh et al., 2015). As for the AMOC, these property transports vary strongly on different timescales, with the meridional heat transport being closely linked to AMOC changes at short timescale (Bryden et al., 2014; Cunningham et al., 2013; Johns et al., 2023).

By producing these datasets for over 20 years, the RAPID array has demonstrated the importance of sustained observing systems for detecting and interpreting changes in the North Atlantic ocean circulation. Other continuous AMOC observing efforts have since been developed, including the SAMBA array at 34.5°S in the South Atlantic (Meinen et al., 2018) and the OSNAP array in the subpolar North Atlantic (Fu et al., 2025). More recently, Fox et al. (2026) introduced SCOTIA, a reconstruction of the subpolar AMOC at OSNAP latitudes that was extended over the 20 years of the RAPID record. Together, these records allow us to compare subtropical and subpolar overturning and to investigate, for example, whether the AMOC varies coherently across latitudes, and over which timescales (Frajka-Williams et al., 2023).

In this context, we document the data products derived from the RAPID array from April 2004 to November 2024, together with the structure, format, and content of the associated data files, to facilitate reuse of the dataset. The data products include the overturning streamfunction and AMOC strength in depth and density coordinates, transports in different oceanic layers, the meridional heat and freshwater transports, and the temperature, salinity and meridional velocity fields used in the calculation. The data products are freely available on the RAPID website: http://www.rapid.ac.uk/. We also introduce the code used to generate these data products to improve transparency and reproducibility. The published code covers the "top level" calculation of the AMOC, streamfunction and derived transports, and requires input data that are also freely available.

https://doi.org/10.5194/essd-2026-922
Preprint. Discussion started: 19 November 2026
© Author(s) 2026. CC BY 4.0 License.



Open Access Earth System Science Data Discussions

We describe the array and method used to derive the data products in Sect. 2, including updates on the method since the last data release in February 2026. The code and data archive are introduced in Sect. 3. In Sect. 4 we discuss the mean, standard deviation and long-term changes of the overturning circulation and property transports, which we place in the context of previous estimates. In particular, we estimate that the linear trend in the AMOC strength is -0.7 ± 0.6 Sv/decade (Fig. 1), and that the linear trends in the meridional heat transport (MHT) and freshwater transport (FWT) are -0.01 ± 0.04 PW/decade and 0.01 ± 0.03 Sv/decade, respectively (Fig. 2). We conclude in Sect. 5 with main open questions that this new release of the data products raises.

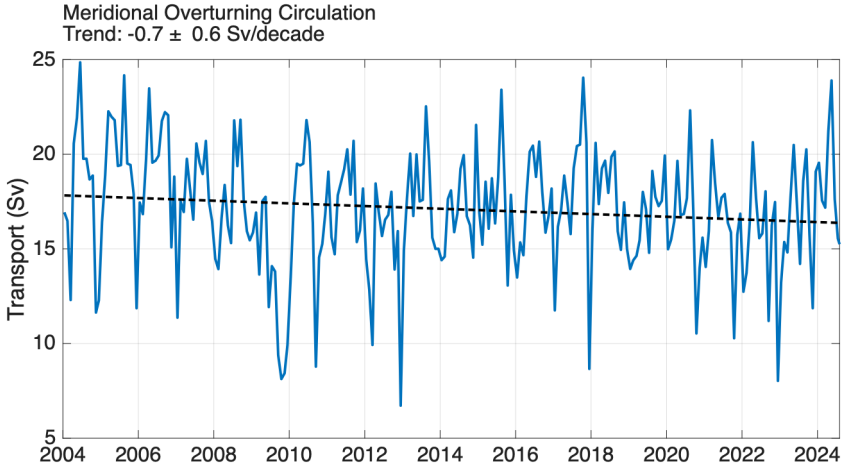


Figure 1: Timeseries and linear trend of the AMOC strength evaluated in depth coordinates from April 2004 to November 2024. The black dashed line indicates the linear trend estimated from the deseasonalised monthly AMOC strength. The trend and its uncertainty are given in the title when assuming independent residuals. Table 2 gives the uncertainty estimates when assuming independent residuals and when considering the autocorrelation of successive months.

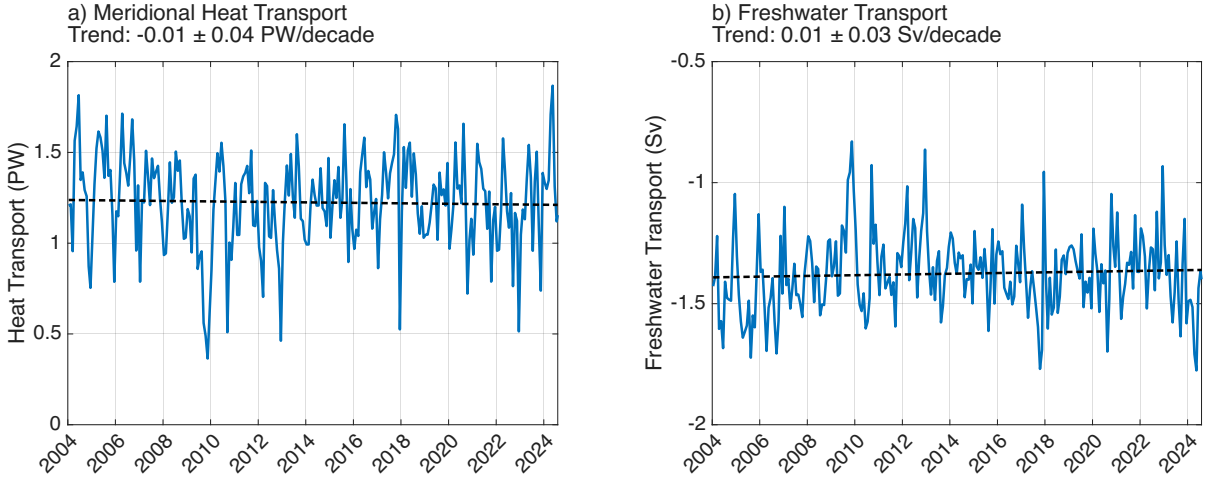


Figure 2: Timeseries and linear trends of the (a) MHT and (b) FWT from April 2004 to November 2024. The black dashed lines indicate the linear trends estimated from the deseasonalised monthly MHT and FWT. The trends and their uncertainties are given in the titles when assuming independent residuals. Table 2 gives the uncertainty estimates when assuming independent residuals and when considering the autocorrelation of successive months.

https://doi.org/10.5194/essd-2026-922
Preprint. Discussion started: 19 November 2026
© Author(s) 2026. CC BY 4.0 License.



Open Access Earth System Science Data Discussions

2 Material and Methods

This section provides an overview of the methods used to derive the RAPID dataset. All methods have been described in detail in previous publications referenced below and are only briefly summarized here. Further details can be found in the relevant references.

2.1 The Endpoint Method for Deriving RAPID Dataset

The endpoint method combines various transport profiles derived from the RAPID array data to produce the overturning streamfunction evaluated in depth coordinates, as described by McCarthy et al. (2015) and Petit et al. (2025). The four main components are (1) the transport through the Florida Straits (Meinen et al., 2010; Volkov et al., 2024), (2) the Ekman transport (Hersbach et al., 2020), (3) the transport within the Bahamas escarpment offshore Abaco Island (Johns et al., 2008), and (4) the internal geostrophic transport between the eastern and western boundaries of the RAPID array (Johns et al., 2005).

Funded by the NOAA Office of Climate Observations, the Florida Straits transport estimates are based on electromagnetic cable measurements (Baringer & Larsen, 2001; Larsen, 1992) and data from repeated hydrographic sections across the Florida Straits, both freely available on the NOAA AOML's website: https://www.aoml.noaa.gov/phod/wbts/. The cable record since 2000 was recently corrected for the secular change in the geomagnetic field (Volkov et al., 2024). Unfortunately, cable measurements were interrupted in November 2023 due to a mechanical failure. Since then, the gaps in the cable record have been filled using a combination of satellite altimetry and bottom pressure measurements from gauges deployed on both sides of the Florida Straits. This approach provides a reliable alternative for monitoring Florida Current transport while efforts to restore the cable system are underway (Volkov et al., 2025).

Ekman transport is derived from the ERA5 reanalysis estimates of wind stress (Hersbach et al., 2020), which are available on the Copernicus website: https://doi.org/10.24381/cds.adbb2d47. For RAPID calculations, this transport is distributed uniformly over the upper 100-m depth of water.

Near the western boundary, the transport over the Bahamas escarpment, commonly refer to as the Western Boundary Wedge (WBW), is estimated from six tall moorings equipped with point and profiling acoustic Doppler current meters, as described in Johns et al. (2008). East of the escarpment, an internal geostrophic transport is calculated between the western and eastern boundaries of the RAPID array. At each of these boundaries, a dynamic height profile is derived by concatenating mooring data vertically with a reference level of 4820 dbar. Note that the calibration of the moored instruments and the processing of the corresponding measurements are performed consistently by a single group using a standardized method (McCarthy et al., 2015). The individual records of all moored instruments deployed since the instalment of the RAPID array can be downloaded from the British Oceanographic Data Centre (BODC) website: https://www.bodc.ac.uk/resources/inventories/edmed/report/6156/. Each of the merged profiles is then mapped onto a regular depth grid (Johns et al., 2005) and extrapolated above the shallowest instrument at ~100-m depth (McCarthy et al., 2015). A time-invariant transport profile is added to the internal geostrophic transport profile below 4820 dbar, which represent the

https://doi.org/10.5194/essd-2026-922
Preprint. Discussion started: 19 November 2026
© Author(s) 2026. CC BY 4.0 License.



Antarctic Bottom Water (AABW) transport (Frajka-Williams et al., 2011). Finally, a compensation transport profile is added to the internal geostrophic profile so that there is no net meridional transport when the four transport components are summed (Kanzow et al., 2007).

The combination of these four transport profiles yields a basin-wide transport profile and associated overturning streamfunction in depth coordinates. The AMOC strength in depth coordinates ($AMOC_z$) is estimated as the maximum of the overturning streamfunction at every time step in a depth range of 200–2000 m (Cunningham et al., 2007). A decomposition of the transport in different layers is also derived from the basin-wide transport profile (Table 1). For example, the upper mid-ocean transport is defined as the sum of interior and WBW transports integrated from the surface down to the depth of the streamfunction maximum. These transports are estimated at daily time steps and provided as monthly averages. The AMOC strength in depth space is also provided as 5-day averages, which resolve variability down to the 10-days timescale, the shortest timescale on which oceanic adjustment maintains mass balance across the RAPID section (Kanzow et al., 2007). All transports are positive northward and given in Sv (10^6 m^3/s).

2.2 The 2D Method for Deriving RAPID Dataset

The two-dimensional (2D) method used to derive the AMOC strength in density coordinates as well as the MHT and FWT is described in detail by Smeed et al. (2026) and is briefly summarized here. The calculation of these quantities requires spatially continuous estimates of gridded temperature, salinity and meridional velocity across the whole basin at 26°N. Therefore, the 2D method requires the use of ancillary data in the ocean interior that cannot be obtained from the moorings alone.

In the Florida Straits, gridded temperature and salinity fields are derived from repeat hydrographic sections following the method described by Johns et al. (2023), and velocities are directly measured by SADCP/LADCP measurements at nine stations across the Straits.

Over the Bahamas escarpment, the transport is derived from the mooring temperature and salinity profiles in the same way as in the endpoint method. The density in this region is then derived from the mooring temperature and salinity profiles.

In the ocean interior above 1800 dbar, gridded temperature and salinity fields are derived from an Objective Analysis (OA) of Argo and mooring profiles. The OA includes all profiles at 26.5°N within a 10-day window and uses an isotropic Gaussian function with a 500 km length scale to weights data. Below 1800 dbar and west of 74°W, the gridded fields are derived from the WBTS (https://www.aoml.noaa.gov/ftp/phod/WBTS/Global_Class/) and GO-SHIP A05 (https://cchdo.ucsd.edu/search?expanded=true&query=A05) sections interpolated in time. Below 1800 dbar and east of 74°W, the gridded fields are derived from the World Ocean Atlas (WOA2023) database (https://www.ncei.noaa.gov/products/world-ocean-atlas) and are set constant in time based on their 1991–2020 mean. The gridded meridional velocity is then calculated using geostrophy at each longitude with dynamic height profiles referenced to 1760 dbar east of 74°W and to 800 dbar west of 74°W, for consistency with previous approaches (Biló & Johns, 2020; Meinen et al., 2019). The final gridded fields in the ocean interior are estimated on a longitude grid of 0.25° resolution from 76.75°W to 14°W, and on a pressure grid of 20 dbar resolution from the surface to 6120 dbar.

https://doi.org/10.5194/essd-2026-922
Preprint. Discussion started: 19 November 2026
© Author(s) 2026. CC BY 4.0 License.



Once calculated for each of the three regions (WBW, Florida Straits and ocean interior) at 10-day time steps, which is a time constraint inherited from the Argo array, velocities are integrated in density bins from the surface to derive a profile of accumulated transport at each longitude of the gridded field. The interior transport is estimated by combining geostrophic and Ekman velocities, as well as a zonally uniform adjustment so that the total transport profile matches that determined by the endpoint method, which also ensures that there is no total net transport. Profiles of accumulated transport are then summed across all longitudes and averaged monthly to obtain the overturning streamfunction as a function of potential density at monthly time steps. The RAPID dataset provides the overturning streamfunction evaluated in potential density relative to surface (σ_0-space) and to 2000 dbar (σ_2-space). The AMOC in density coordinates ($AMOC_{\sigma 0}$ and $AMOC_{\sigma 2}$) is then calculated as the maximum of the overturning streamfunction for densities higher than $\sigma_0 = 27$ kg m^{-3} and $\sigma_2 = 36$ kg m^{-3} to avoid capturing the upper subtropical gyre cell identified by Smeed et al. (2026). Therefore, the AMOC strength is representative of the deep overturning cell at all times.

In addition to these products, the RAPID dataset provides the MHT (Johns et al., 2011) and FWT (McDonagh et al., 2015) at each time step from the gridded property and velocity fields. The MHT is estimated by integrating the Ekman and geostrophic velocities multiplied by conservative temperature over the section area, which is then scaled by the specific heat capacity. The FWT is estimated by integrating the sum of Ekman, geostrophic and barotropic velocities over the section area. To close the salt budget, a spatially uniform barotropic velocity is added so that the total salt transport balances the Beiring Strait salt import.

2.3 Latest Updates on the Methods

The RAPID data version v2024-2 was generated by using the endpoint and 2D methods described above, and includes some methodological changes as compared to the previous release published in February 2026 (v2024-1a). These changes are listed below:

- **Change in the endpoint method on the latitude used for geostrophic calculation**. As data are no longer collected at the Mid-Atlantic Ridge, we now use a latitude of 26.5°N instead of 25.7°N that is more representative of the whole section and makes the calculation more consistent with the 2D method.
- **Change in the endpoint method to derive the western boundary profile** (Fig. A1). Previously, the dynamic height on the western boundary was calculated by concatenating data from moorings WB3 (c. 4840 m), WBH2 (c. 4740 m) and WB2 (c. 3920 m), relative to a reference level of 4820 dbar (4735 m). Inshore of WB2, transport at each depth was estimated from velocity measurements at moorings WB2, WB1, WB0 and WBADCP. However, on three occasions (2005-2006, 2018 and 2023, about 12 months in all) the WB2 mooring collapsed or could not be deployed. In these periods, the western dynamic height was calculated from WB3 alone, and transport inshore of WB3 was estimated from velocity measurements at WB3, WBH2, WB1, WB0 and WBADCP. Thus, the western dynamic height and western boundary wedge variables had slightly different definitions depending on whether WB2 was available. In the new calculation: 1) the dynamic height on the western boundary is always a concatenation of dynamic height at WB2 (above 3920 m) and WB3 (below 3920 m); 2) the western boundary wedge transport is always the

https://doi.org/10.5194/essd-2026-922
Preprint. Discussion started: 19 November 2026
© Author(s) 2026. CC BY 4.0 License.



transport inshore of WB2 above 3920 m and the transport inshore of WB3 below 3920 m; 3) the reference level transport at 3920m between WB2 and WB3 is explicitly estimated from the current meter data from WB2, WBH2 and WB3; and then 4) the total transport is the sum of the transports calculated from the concatenated dynamic height profile, the western boundary wedge and a reference level transport applied at and above 3920 m. When WB2 data are unavailable, the transport inshore of WB2 and between WB2 and WB3 is estimated from current meter data at WBADCP, WB0, WB1, WBH2 and WB3. The dynamic height at WB2 is then estimated by correcting the WB3 dynamic height for the transport between WB2 and WB3. Therefore, this change in the endpoint method ensures consistency of the dynamic height definitions on the western boundary throughout the whole time series, regardless of whether WB2 data are available. These changes have only a minor impact on the AMOC but significantly reduce the mean compensation transport, as the barotropic transport between WB2 and WB3 was previously included in it.

- **Change to the Ekman transport calculation.** The ERA5 wind stress is now averaged from 8 values per day instead of 4, and the longitude range over which we extract these values have been extended to 14°W.
- **Change to the estimation of Florida Straits transport.** The Florida Straits transport is now estimated by combining high-frequency sea level variability measured by bottom pressure gauges on opposite sides of the Florida Current with low-frequency variability derived from satellite altimetry. Satellite data are used to correct pressure gauge records for sensor offsets and drifts while preserving high-frequency signals. The resulting cross-stream sea level differences are converted into Florida Current volume transport estimates using a linear relationship calibrated against submarine cable measurements (Volkov et al., 2025). Note that this change applies to the last year of the AMOC record, after the cable fault in November 2023, and to fill in some prior short gaps in the cable record.
- **Change to the estimation of the AMOC strength in density space.** The AMOC in density coordinates is now calculated as the maximum of the overturning streamfunction over a specific density range ($\sigma_0 > 27$ kg m^{-3} and $\sigma_2 > 36$ kg m^{-3}) to avoid capturing the upper subtropical gyre cell identified by Smeed et al. (2026). Therefore, the AMOC strength is now representative of the deep overturning cell at all times.
- **Change in the time resolution of the RAPID timeseries.** The overturning and associated transport timeseries are now only provided at monthly timescale, as well as at 5-day timescale for the overturning streamfunctions and the AMOC in depth space, without any filtering applied.

3 Code and Data Archive

3.1 Description of the Code

The code is written in PYTHON, translated from the MATLAB code previously used to produce the dataset, and is released under the GNU General Public License v3.0. It is organised in three parts, each with its own version number and Zenodo DOI (Fig. 3):

https://doi.org/10.5194/essd-2026-922
Preprint. Discussion started: 19 November 2026
© Author(s) 2026. CC BY 4.0 License.



Open Access Earth System Science Data Discussions

- *rapid-1d-python* (https://doi.org/10.5281/zenodo.23216772) calculates the overturning streamfunction and AMOC in depth space, transport profiles and water-mass layer transports at daily resolution. Its inputs are the dynamic height and western boundary wedge profiles from the moorings, the Florida Current, Ekman and Antarctic Bottom Water transports, and the interior cell areas.
- *rapid-2d-python* (https://doi.org/10.5281/zenodo.23217145) calculates the overturning streamfunction and AMOC in density spaces ($AMOC_{\sigma 0}$ and $AMOC_{\sigma 2}$), as well as the MHT and FWT, every 10 days. Its input is the gridded property and velocity fields of the section (*rapid_2D_product_<version>.nc*), with Florida Strait corrections.
- *rapid-amoc-python* (https://doi.org/10.5281/zenodo.23217740) averages the results of both to monthly means, and also to 5-day means for the AMOC and overturning streamfunction in depth space, and writes the published files. The AMOC strength is derived from the averaged overturning streamfunctions.

The code therefore requires input files, which can be found in a Zenodo archive: https://doi.org/10.5281/zenodo.23363394. The upstream MATLAB processing that produces these files from the datasets described in Sect. 2.1 and 2.2 is not included in this release, and will be translated and published in a later release.

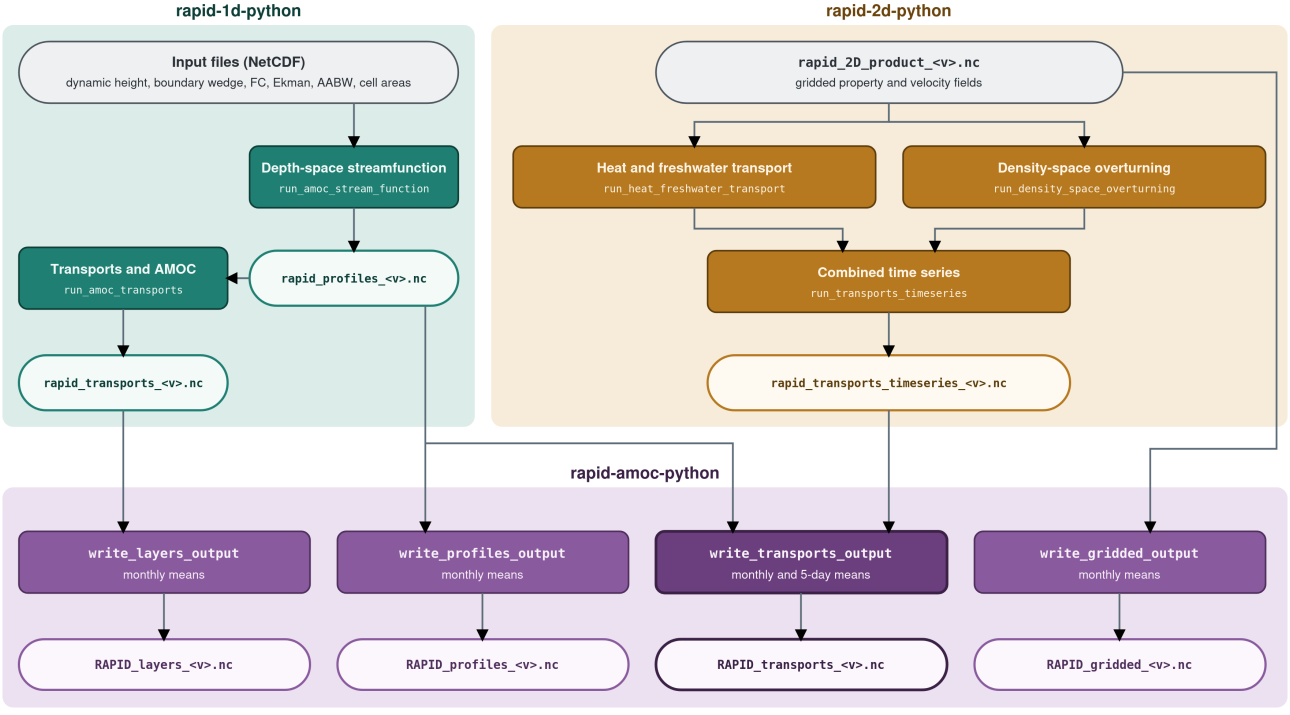


Figure 3. Structure of the RAPID code. *rapid-1d-python* (green) and *rapid-2d-python* (orange) process the input files (grey), and *rapid-amoc-python* (purple) averages and combines their results into the published files. Rectangles are processing steps, labelled with the PYTHON function that runs them. Rounded boxes are files with <v> being the dataset version. FC: Florida Current; AABW: Antarctic Bottom Water. The Florida Strait correction files read by *rapid-2d-python* are not shown.

https://doi.org/10.5194/essd-2026-922
Preprint. Discussion started: 19 November 2026
© Author(s) 2026. CC BY 4.0 License.


All settings are held in a YAML configuration file for each part, named with the dataset version. The configuration lists each input file with its SHA-256 checksum, so that a user can check that they are running the published inputs. The Zenodo record of *rapid-amoc-python* (https://doi.org/10.5281/zenodo.23217740) holds all three parts in a single archive. After installing the PYTHON packages listed in its *requirements.txt* and placing the input files as described in its *RELEASE.md*, one script (*demo_scripts/run_full_pipeline.py*) runs all three parts and writes the output files. Each published file records in its global attributes the dataset version and the DOIs of the three code releases that produced it. The RAPID code v0.1.0 is used to generate the RAPID dataset version v2024-2. A new code release will be made with each dataset version.

3.2 Data Archive

The RAPID dataset generated by the RAPID code v0.1.0 is freely available for download from the RAPID website: http://www.rapid.ac.uk/. The dataset is organised in four files (Table 1) and combine products derived by the methods described in Sect. 2:

- *RAPID_gridded_v2024-2.nc* contains the gridded temperature, salinity and meridional velocity fields across the RAPID array section derived from the 2D method at monthly timescale. The meridional velocity field contains three individual components: the geostrophic velocity field derived from in-situ measurements and geostrophic balance, the Ekman velocity field at surface derived from ERA5 reanalysis, and a spatially uniform scalar representing the net meridional velocity derived from salt and mass conservation at every time steps. Note that the sizes of the grid cells vary with depth, and velocity should be multiplied by the area provided in this file to obtain the meridional transport in each cell.
- *RAPID_transports_v2024-2.nc* contains (1) the overturning streamfunction and associated AMOC transports evaluated in depth coordinates, which are derived from the end-point method; (2) the overturning streamfunction and associated AMOC transports evaluated in potential density coordinates, for potential density referenced to the surface and to 2000 dbar, which are derived from the 2D method; and (3) the MHT and FWT derived from the gridded properties and velocity fields at 26°N. These products are derived at monthly timescale from April 2004 to November 2024, except for the AMOC transport evaluated in depth coordinates that is also derived at 5-day timescale.
- *RAPID_layers_v2024-2.nc* contains the meridional transports in different layers across the RAPID array, which are derived from the end-point method at monthly timescale.
- *moc_error.nc* contains estimates of AMOC uncertainty when evaluated in depth coordinates. The error timeseries varies with time and is estimated using the methodology described by McCarthy et al. (2015), which accounts for the accuracy of the moored instruments and systemic uncertainties associated with the other components of the total transport. The current timeseries extends to October 2015, and an updated version is currently being developed by the RAPID team.

https://doi.org/10.5194/essd-2026-922
Preprint. Discussion started: 19 November 2026
© Author(s) 2026. CC BY 4.0 License.



Further details on the data files and the changes made between successive dataset releases are provided in the accompanying *ReadMe.txt* file. In addition to the datasets available through the RAPID website, the RAPID team can provide further products to support specific user needs.

Table 1: Overview of the RAPID dataset version v2024-2 described in this paper and freely available on the RAPID website: http://www.rapid.ac.uk/.

File name	Content	Format	Status	Accessibility
RAPID_gridded_v2024-2.nc	• *area*: Area of grid cell (m^2) • *CT_1m*: Conservative Temperature (°C) • *SA_1m*: Absolute Salinity (g/kg) • *V_insitu_1m*: Geostrophic Velocity (m/s) • *V_ekman_1m*: Ekman Velocity (m/s) • *V_net_1m*: Net Meridional Velocity (m/s)	NetCDF	Up to date	Open Access
RAPID_transports_v2024-2.nc	• *stream_depth_1m*: Streamfunction in depth space at monthly intervals (Sv) • *amoc_depth_1m*: AMOC in depth space at monthly intervals (Sv) • *stream_depth_5d*: Streamfunction in depth space at 5-day intervals (Sv) • *amoc_depth_5d*: AMOC in depth coordinates at 5-day intervals (Sv) • *stream_sigma0_1m*: Streamfunction in σ_0-space at monthly intervals (Sv) • *amoc_sigma0_1m*: AMOC in σ_0-space at monthly intervals (Sv) • *stream_sigma2_1m*: Streamfunction in σ_2-space at monthly intervals (Sv) • *amoc_sigma2_1m*: AMOC in σ_2-space at monthly intervals (Sv) • *heat_trans_1m*: Meridional heat transport at monthly intervals (PW) • *frwa_trans_1m*: Meridional freshwater transport at monthly intervals (Sv)	NetCDF	Up to date	Open Access

https://doi.org/10.5194/essd-2026-922
Preprint. Discussion started: 19 November 2026
© Author(s) 2026. CC BY 4.0 License.



RAPID_layers_v2024-2.nc	• *trans_FC_1m*: Transport through the Florida Strait at monthly intervals (Sv) • *trans_UMO_1m*: Upper Mid-Ocean transport at monthly intervals (Sv) • *trans_ekm_1m*: Ekman transport at monthly intervals (Sv) • *trans_the_1m*: Surface water (z < 800 m) transport at monthly intervals (Sv) • *trans_aiw_1m*: Intermediate water (800 m < z < 1100 m) transport at monthly intervals (Sv) • *trans_ud_1m*: Upper deep water (1100 m < z < 3000 m) transport at monthly intervals (Sv) • *trans_ld_1m*: Lower deep water (3000 m < z < 5000 m) transport at monthly intervals (Sv) • *trans_bw_1m*: Bottom water (z > 5000 m) transport at monthly intervals (Sv) • *trans_comp_1m*: Compensation transport at monthly intervals (Sv)	NetCDF	Up to date	Open Access
moc_error.nc	Error on the AMOC in depth space at 12-hourly intervals. Times are in days since 1st April 2004.	NetCDF	Up to October 2015	Open Access

4 Results and Discussions: Long-Term Trend Analysis

With more than 20 years of continuous observations, the RAPID dataset provides a unique opportunity to investigate long-term changes in ocean properties and circulation at 26°N. Here, we consider not only the AMOC metric, but also other key diagnostics of ocean change, including the property transports. Throughout the section, we provide the mean, standard deviation and trend estimates of each timeseries (Table 2). Trends are estimated from deseasonalised monthly timeseries using the ordinary least squares (OLS) method. Table 2 gives two estimates of trend uncertainty, both expressed as 95% confidence intervals that are calculated as the standard error of the slope multiplied by the 97.5th percentile of a Student t distribution. The first estimate uses the standard OLS error, which assumes independent residuals (i.e. white noise model), for consistency with previously published values, and is computed with $N - 2$ degrees of freedom, where N is the number of months (248). The second estimate accounts for the autocorrelation of successive months by replacing N with an effective sample size $N^* = N\Delta t/T$, where Δt is one month and T is the integral timescale of the OLS residuals, estimated from their autocovariance function (Thomson & Emery, 2014). An evaluation of the most appropriate noise model for assessing the trend significance in more details would require a dedicated analysis and is beyond the scope of this study.

https://doi.org/10.5194/essd-2026-922
Preprint. Discussion started: 19 November 2026
© Author(s) 2026. CC BY 4.0 License.



Open Access Earth System Science Data Discussions

Table 2: Summary of the mean, standard deviation and trends for the RAPID timeseries version v2024-2 described in this paper. Trends are estimated from deseasonalised monthly timeseries using OLS, the uncertainty being estimated using a white noise model (white) and an effective number of degrees of freedom (edof).

	Mean	Standard Deviation	Trend (white)	Trend (edof)
$AMOC_z$	17.10 Sv	3.15 Sv	-0.7 ± 0.6 Sv/dec	-0.7 ± 0.9 Sv/dec
Ekman Transport	3.48 Sv	2.04 Sv	0.1 ± 0.4 Sv/dec	0.1 ± 0.5 Sv/dec
Florida Transport	31.66 Sv	2.16 Sv	-0.1 ± 0.4 Sv/dec	-0.1 ± 0.5 Sv/dec
UMO	-17.88 Sv	2.80 Sv	-0.8 ± 0.5 Sv/dec	-0.8 ± 1.1 Sv/dec
UDW	-11.99 Sv	1.59 Sv	-0.2 ± 0.3 Sv/dec	-0.2 ± 0.3 Sv/dec
LDW	-5.98 Sv	2.16 Sv	0.8 ± 0.4 Sv/dec	0.8 ± 0.7 Sv/dec
MHT	1.22 PW	0.25 PW	-0.01 ± 0.04 PW/dec	-0.01 ± 0.08 PW/dec
FWT	-1.38 Sv	0.16 Sv	0.01 ± 0.03 Sv/dec	0.01 ± 0.05 Sv/dec

4.1 Long-Term Changes in Overturning Circulation

We first examine the overturning circulation, its mean, variability and 20-year trend. The overturning streamfunction evaluated in depth (ψ_z) and density (ψ_σ) coordinates are shown in Figure 4, for potential density referenced to 2000 dbar. As discussed by Smeed et al. (2026), the overturning streamfunction in density coordinates (Fig. 4b) reveals a shallow overturning cell representing the subtropical gyre circulation (Berglund et al., 2022; Tooth et al., 2024), which is obscured when evaluated in depth coordinates (Fig. 4a). Therefore, the trends in accumulated transports exhibit different shapes when evaluated in depth or density coordinates. The negative trend in ψ_z only reflects a weakening of the main overturning cell (Fig. 4c), while the trend in ψ_σ also reveals a strengthening of the shallow overturning cell, and thus a strengthening of the southward recirculation of upper water within the subtropical gyre (Fig. 4d).

The monthly variability of the overturning streamfunction is shown in Fig. 4 (e-f) together with the time variability of Z_{moc}, the depth at the maximum of ψ_z, and σ_{moc}, the density at the maximum of ψ_σ within the main overturning cell. The monthly variability of Z_{moc} and σ_{moc} is relatively small (standard deviations: 115 m and 0.07 kg m^{-3}, respectively) around their climatological mean of 1001 m and 36.66 kg m^{-3}. Furthermore, we do not find a significant trend in both Z_{moc} and σ_{moc} (not shown). This is consistent with Fox et al. (2026) at the SCOTIA line, although the two estimates are not directly comparable because they used neutral density instead of σ_2 coordinates.

The maximum of the overturning streamfunction is used to define the AMOC strength. The mean and monthly standard deviation of the AMOC strength is 17.10 ± 3.15 Sv when derived in depth coordinates, 17.54 ± 3.17 Sv when derived in σ_0 coordinates and 17.66 ± 3.16 Sv when derived in σ_2 coordinates (Fig. A2). The close agreement between these values is consistent with Smeed et al. (2026) who showed that the mean and monthly variability of $AMOC_z$, $AMOC_{\sigma 0}$ and $AMOC_{\sigma 2}$ are very close.

https://doi.org/10.5194/essd-2026-922
Preprint. Discussion started: 19 November 2026
© Author(s) 2026. CC BY 4.0 License.

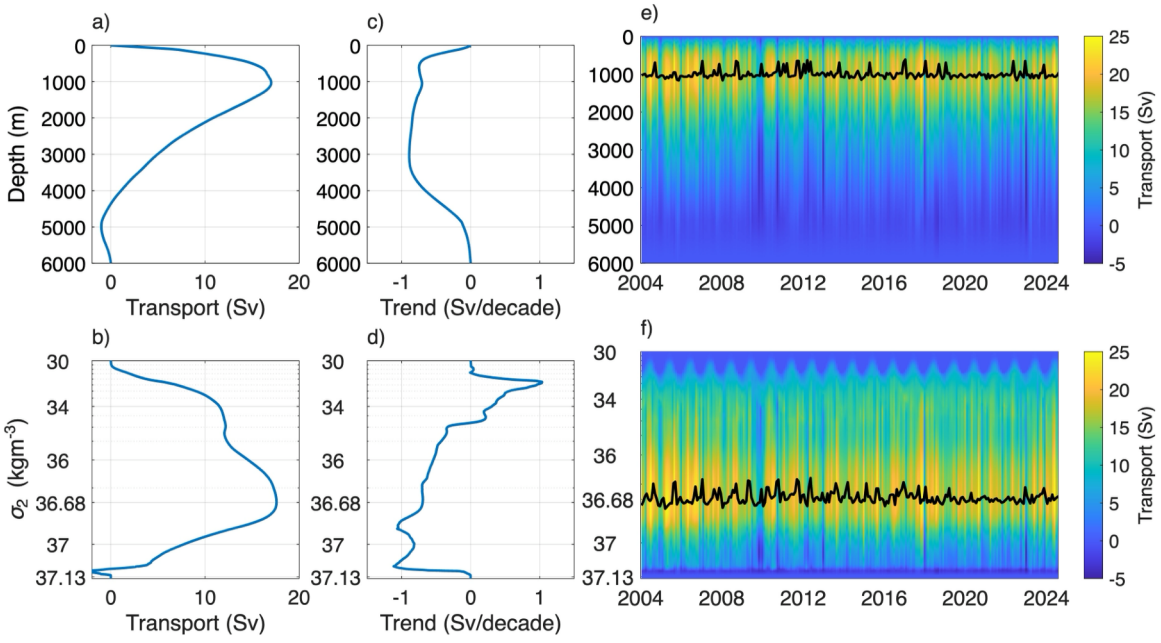


Figure 4: Overturning streamfunction at 26°N, (a, b) its climatological mean, (c, d) its linear trend and (e, f) its monthly evolution when evaluated in (a, c, e) depth and (b, d, f) density coordinates. Black lines indicate the depth (z_{moc}) and density (σ_{moc}) at the maximum of the overturning streamfunction. Note the decimal logarithmic axis used for the overturning streamfunction in density coordinates to better resolve the transport below the thermocline.

The linear trend of $AMOC_z$ is shown in Fig. 1, estimated by OLS regression on the deseasonalised monthly timeseries. From April 2004 to November 2024, $AMOC_z$ exhibit a declining trend of -0.7 ± 0.6 Sv/decade, which is statistically significant when assuming independent residuals (Table 2). The trends in $AMOC_{\sigma 0}$ and $AMOC_{\sigma 2}$ are identical to the one in $AMOC_z$, indicating that evaluating the AMOC in depth or density coordinates has no impact on its linear trend at 26°N. The trend estimate is consistent with previous studies reporting a significant decline of the AMOC at 26°N (Smeed et al., 2014, 2018; Volkov et al., 2024; Xing et al., 2026). The differences between our trend estimate and those reported by these previous studies is mainly explained by different record lengths. Fig. 5a shows the evolution of the linear trend as the RAPID record lengthens from the start of the timeseries in April 2004. By April 2014, after 10 years of observations, the AMOC trend was negative and significantly different from zero within uncertainties, at -3.1 ± 1.8 Sv/decade. However, the AMOC trend evolved further as the record lengthened, becoming non-significant by December 2017. Yet, after about 18 years of observations (ending in January 2022), the AMOC exhibited again a negative trend that remained significantly different from zero until November 2014. Compared with the previous data release, we note that extending the timeseries by only a few months, from February 2024 to November 2024, is sufficient to weaken the AMOC trend by ~0.2 Sv/decade. The evolution of these trends as the record lengthens highlights the importance of sustained observations: it is only after approximately 15 years that the AMOC trend began to stabilize, emphasizing that long records are needed to robustly identify long-term changes in overturning circulation.

https://doi.org/10.5194/essd-2026-922
Preprint. Discussion started: 19 November 2026
© Author(s) 2026. CC BY 4.0 License.



Furthermore, the uncertainty of the AMOC trend for this last data release is ± 0.6 Sv/decade when assuming independent residuals, but this one increase to ± 0.9 Sv/decade when accounting for the autocorrelation of successive months (Table 2), so that the AMOC trend may be regarded as no longer significant at the 95% level. This highlights the need for an in-depth investigation of the full spectrum of variability when assessing the AMOC trend, even from a relatively long record of 20 years.

The AMOC decline observed at 26°N contrasts with AMOC trends reported in the subpolar gyre. At 47°N, Wett et al. (2023) reported a linear trend of the AMOC of 0.03 Sv/year over 1993–2018. Volkov et al. (2026) also reported that there is no significant trend in overturning strength (0.1 ± 0.5 Sv/dec) between 2002 and 2025 at 41°N. Further north, Fox et al. (2026) reported that the linear trend of the AMOC at the SCOTIA line is weak and not statistically significant (0.42 ± 0.80 Sv/decade) over their 20-year record. The difference in AMOC trends between 26°N and these higher latitudes suggests that processes modify or obscure the long-term AMOC signal between the sections, highlighting the value of sustained observations at multiple latitudes. The now longer AMOC timeseries at OSNAP will be valuable for addressing this question and assessing how long-term changes in the AMOC are connected between the subpolar and subtropical gyres.

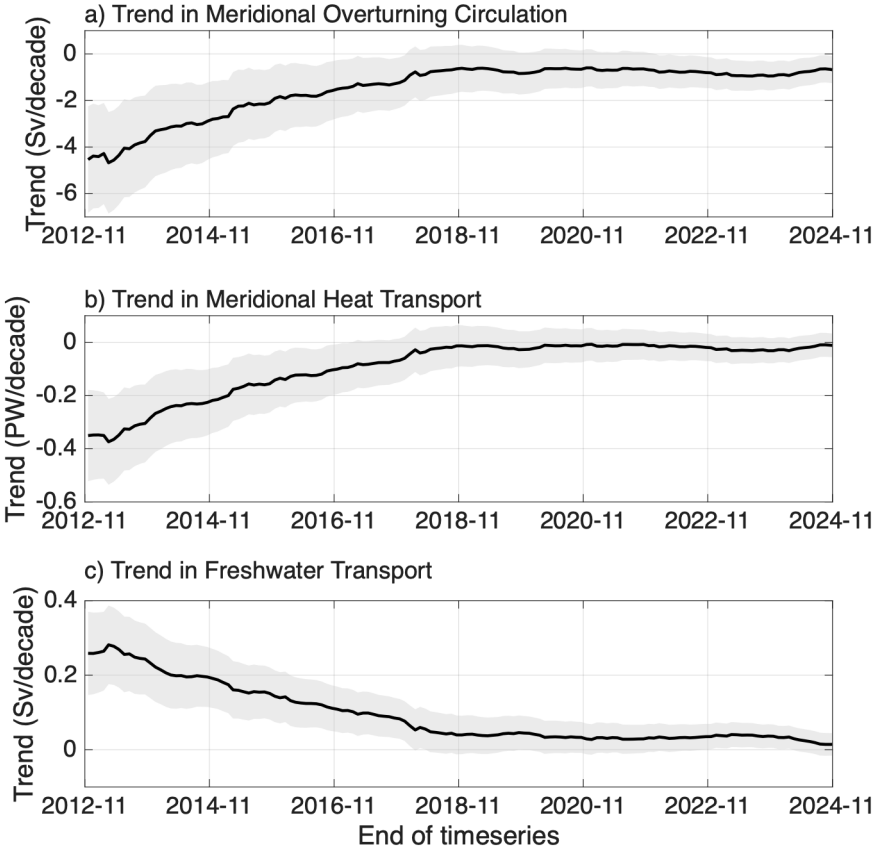


Figure 5: Evolution of the linear trends in (a) $AMOC_z$, (b) MHT and (c) FWT as the record lengthens from its beginning in April 2004. The shaded areas represent the 95% confidence interval for the respective linear trends when assuming independent residuals.

https://doi.org/10.5194/essd-2026-922
Preprint. Discussion started: 19 November 2026
© Author(s) 2026. CC BY 4.0 License.

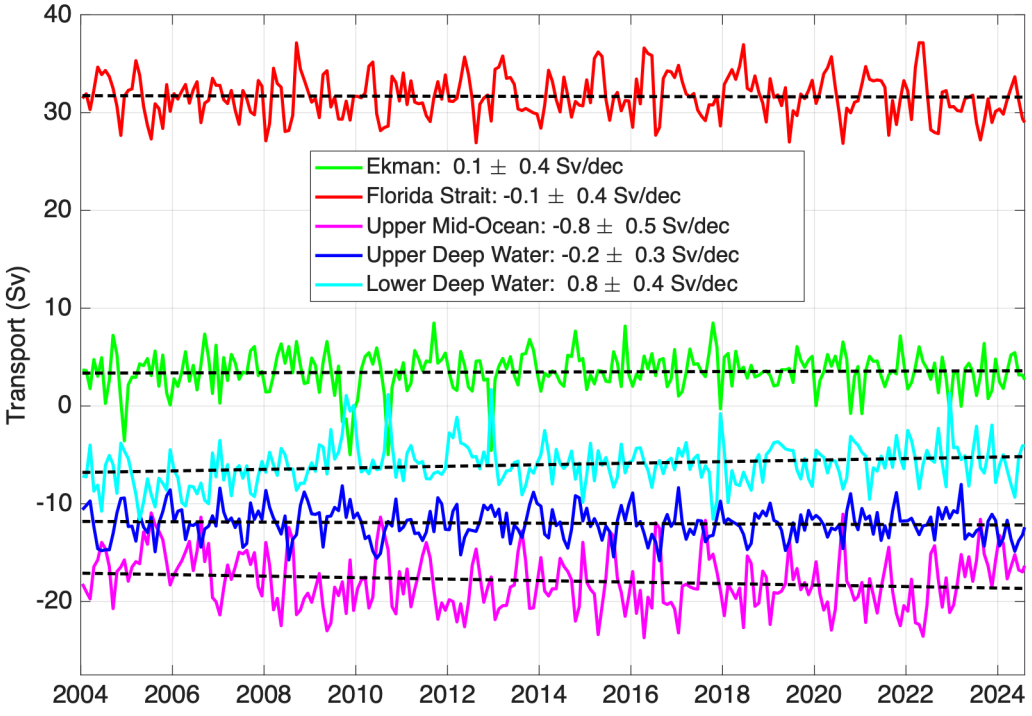


Figure 6: Timeseries and linear trends of the meridional transport in different layers at 26°N from April 2004 to November 2024. The black dashed lines indicate the linear trends estimated from the deseasonalised monthly transports. The corresponding trend estimates and their uncertainties are given in the legend for each component when assuming independent residuals. Table 2 gives the uncertainty estimates when assuming independent residuals and when considering the autocorrelation of successive months.

Fig. 6 shows the decomposition of the meridional transport in different layers that are associated with different water masses at 26°N. Although the Florida Straits transport has remained stable over the 20-year record, as reported by Volkov et al. (2024), the southward Upper Mid-Ocean transport has significantly strengthened with a trend of -0.8 ± 0.5 Sv/decade when assuming independent residuals. At depth, the North Atlantic Deep Water is decomposed into two layers, the Upper Deep Water (UDW at 1100 m < z < 3000 m) and Lower Deep Water (LDW at 3000 m < z < 5000 m). Most of the declining signal is found in the southward LDW (0.8 ± 0.4 Sv/decade), which is significant either when assuming independent residuals or when considering the autocorrelation of successive months (Table 2). This weakening has been shown to be mainly responsible for the weakening of the AMOC lower limb (McCarthy et al., 2025; Smeed et al., 2014). The link between AMOC and LDW changes is also observed further north at the SCOTIA line (Fox et al., 2026).

4.2 Long-Term Changes in Property Transports

We next discuss the mean and long-term changes in temperature, salinity and meridional velocity along the RAPID Array section at 26°N. The 20-year mean fields are shown in Fig. 7, and the linear trends are shown in Fig. 8. Uncertainties on the trends are not shown for these sections, and only strong trends are discussed as likely to be significant. Over most of the

https://doi.org/10.5194/essd-2026-922
Preprint. Discussion started: 19 November 2026
© Author(s) 2026. CC BY 4.0 License.



Open Access Earth System Science Data Discussions

section, the top 1800 m exhibits a warming (Fig. 8a) and salinification (Fig. 8b), which is especially strong above 500 m. As the density in the subtropical gyre is primarily temperature-controlled, these long-term changes result in a decrease in potential density σ_2 for the upper water across the section (Fig. 8c). However, this decrease in density does not lead to a statistically significant change in σ_{moc} over the 20 years of observations, as discussed in Fig 4f. Note that the property trends are close to zero below 1800 m and east of 74°W because the gridded fields are derived from the WOA2023 database and are set constant in time.

The mean meridional velocity in Fig. 7d is close to the one reported by Smeed et al. (2026), which is characterised by a northward Antilles Current at surface and a southward Deep Western Boundary Current (DWBC) at depth over the western boundary. The linear trend in meridional velocity is positive above ~500 m along the western boundary (Fig. 8d). This suggests a strengthening of the northward Antilles Current. However, although we observed a significant declining trend in the southward LDW transport (Fig. 6), the trend below 2000 m is not homogeneously positive along the western boundary, which indicates that the southward DWBC does not weaken uniformly. Further analysis would be required to locate the origin of the LDW decline and test whether most of the LDW trend is carried by the DWBC. The velocity trend in the interior ocean is also difficult to interpret as the signal is relatively weak and varies spatially. Nevertheless, a negative trend above 500 m suggests a net strengthening of the southward recirculation in the subtropical gyre, which would be consistent with the positive trend observed in the shallow overturning cell (Fig 4d).

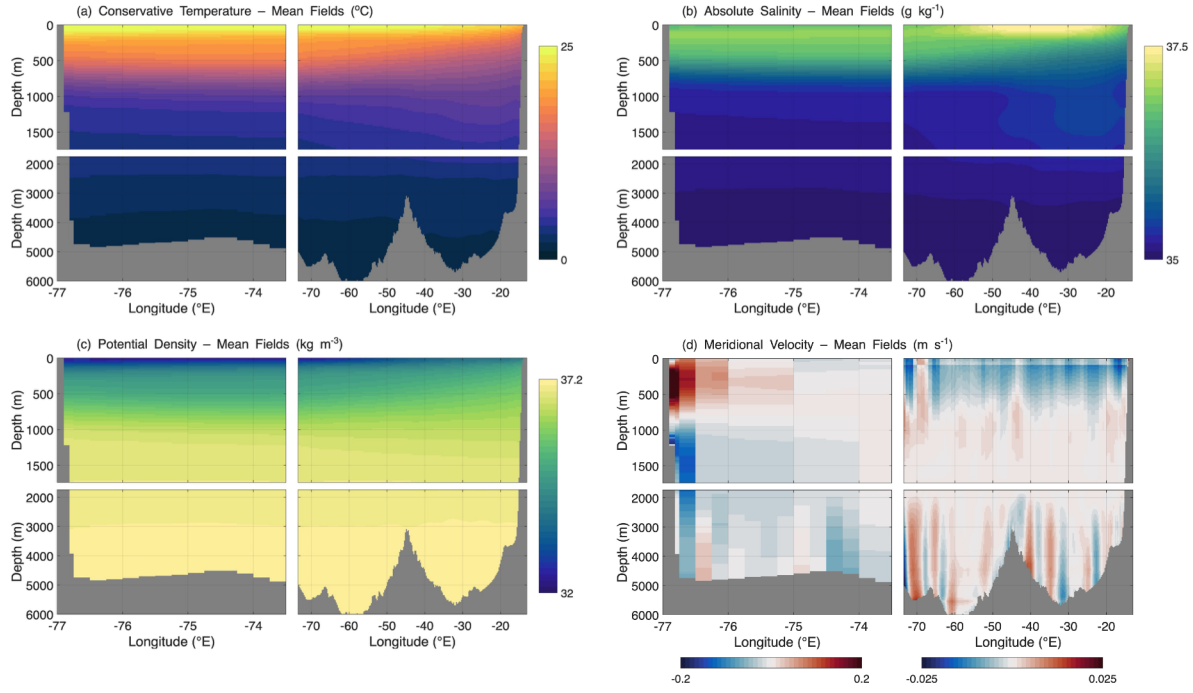


Figure 7: Mean (a) conservative temperature, (b) absolute salinity, (c) potential density σ_2 and (d) meridional velocity east of the Florida Straits from April 2004 to November 2024. Meridional velocity is the combination of geostrophic and Ekman velocities. Note the different colour scale in the plots of meridional velocity between east and west of 73.5°W. Meridional velocity is positive northward.

https://doi.org/10.5194/essd-2026-922
Preprint. Discussion started: 19 November 2026
© Author(s) 2026. CC BY 4.0 License.

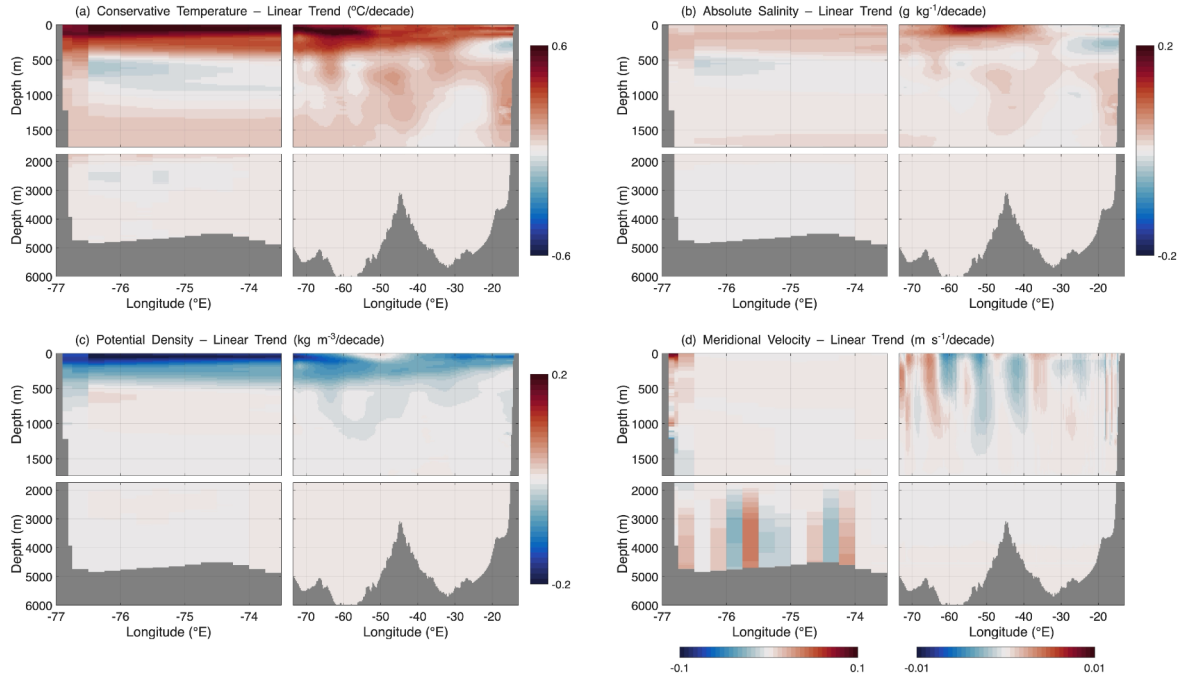


Figure 8: Linear trends in (a) conservative temperature, (b) absolute salinity, (c) potential density σ_2 and (d) meridional velocity east of the Florida Straits. Meridional velocity is the combination of geostrophic and Ekman velocities. Note the different colour scale in the plots of meridional velocity between east and west of 73.5°W. Positive trends indicate warming, salinification, densification and an increase in northward velocity.

The long-term changes in MHT and FWT (Fig. 2) are now examined based on the property and velocity fields described above. Contrary to the AMOC, the 20-year trends in MHT and FWT are close to zero and not statistically significant whether assuming independent residuals or considering the autocorrelation of successive months, with values of -0.01 ± 0.04 PW/decade and 0.01 ± 0.03 Sv/decade, respectively (Table 2). The absence of a significant trend in MHT is consistent with Calafat et al. (2025) who showed no statistically significant trend in MHT at 26°N (0.09 PW/decade with a 95% confidence interval of [−0.03, 0.22]). Their estimation was done by using Bayesian statistical methods applied to multiple observational datasets over a relatively long time period (2004–2020). These near-zero trends in MHT are also consistent with those reported by Fox et al. (2026) at the SCOTIA line over their 20-year record.

As for the AMOC strength, the trends in MHT and FWT are strongly impacted by the length of the timeseries used for their estimations, and their significance remains debated when estimated from short instrumental records (Thresher et al., 2026). Indeed, Fig. 5b and 5c show that the MHT and FWT trends were significantly larger in magnitude than their 20-year trends and different from zero within their uncertainty after only 10 years of observations, with -0.24 ± 0.14 PW/decade and 0.20 ± 0.10 Sv/decade, respectively. However, both the MHT and FWT trends became close to zero and non-significant when the timeseries extended to November 2016 and January 2015, respectively. The strong sensitivity of these linear trends to the record length reveals the importance of sustained observations to robustly identify long-term changes not only in AMOC strength but also in MHT and FWT.

https://doi.org/10.5194/essd-2026-922
Preprint. Discussion started: 19 November 2026
© Author(s) 2026. CC BY 4.0 License.

Open Access Earth System Science Data Discussions

5 Conclusions

Over the last two decades, the RAPID array has provided the longest records of the overturning circulation and property transport in the Atlantic. Used by researchers, forecasting centres, policymakers, and international climate assessment, these data products have and continue to improve our understanding of AMOC variability and long-term changes. This study provides a description of the RAPID code and associated RAPID datasets, and presents the 20-year mean, variability and linear trends of the timeseries from April 2004 to November 2024. By making the code openly available and by documenting the processing steps, this study supports the reproducibility and future use of long-term AMOC observational datasets, building on recent community efforts (Foukal et al., 2026). Together, these efforts can help establish common protocols, facilitating the comparison of measurements across observing arrays.

Beyond documenting the updated timeseries, we raise new questions that the dataset now makes possible to address in future studies. One of the key open questions is the discrepancy between the AMOC and MHT trends. This question is particularly important because the MHT is expected to be a more climatically relevant property than the AMOC (Johns et al., 2023), even though the AMOC has received most of the attention in the past (IPCC, 2021). The discrepancy can be surprising as one might expect the two to be comparable, at least to first order. Indeed, Johns et al. (2023) showed that ~90% of the total MHT at 26.5°N is carried by the zonally averaged overturning circulation at short timescale. However, they also highlight that this relationship weakens on interannual-to-decadal timescales because it is modulated by changes in upper-ocean temperature. In particular, the warming of the Florida Current since 2012 has been identified as offsetting the AMOC decline (Johns et al., 2023). As the MHT depends on the temperature of both the northward Florida Current and the southward upper mid-ocean, it remains to be tested whether the warming of the upper mid-ocean seen in Fig. 8a counteracts the contribution of the warming Florida Current to the total MHT. Nevertheless, model results suggest that the subtropical gyre accounts for only 37% of the total MHT across 26°N (Tooth et al., 2024), so any compensation by the warming of the upper mid-ocean may be limited. Disentangling the drivers of the long-term AMOC–MHT decoupling will require further investigation, and the discussion here can be seen as a starting point.

A related question is whether the AMOC trend observed at 26°N from more than two decades of continuous observations is climatically relevant. McCarthy et al. (2025) addressed this question by using a signal-to-noise framework on the AMOC transport and found that, even when removing the noisy Ekman component, the current AMOC trend would not produce “unfamiliar” or “unknown” AMOC levels until 2040s and 2060s, respectively. Their study highlights a challenge in detecting persistent change in the AMOC, which emphasizes the need for high-quality direct observations such as those provided by the RAPID array since 2004. Only with such observations do we obtain the ground-truth needed to answer the main question of a possible AMOC decline.

https://doi.org/10.5194/essd-2026-922
Preprint. Discussion started: 19 November 2026
© Author(s) 2026. CC BY 4.0 License.



Open Access Earth System Science Data Discussions

Code and Data Availability

All three parts of the RAPID code v0.1.0 are available under a single Zenodo archive at https://doi.org/10.5281/zenodo.23217740. The input files required to run the RAPID code v0.1.0 are available on Zenodo at https://doi.org/10.5281/zenodo.23363394. The RAPID dataset v2024-2 generated by the RAPID code v0.1.0 is accessible for download from the RAPID website: http://www.rapid.ac.uk/ (Moat et al., 2026). The DOI for the RAPID dataset v2024-2 is 10.5285/5c39bf4e-5140-5546-e063-7086abc027bc.

Appendix A

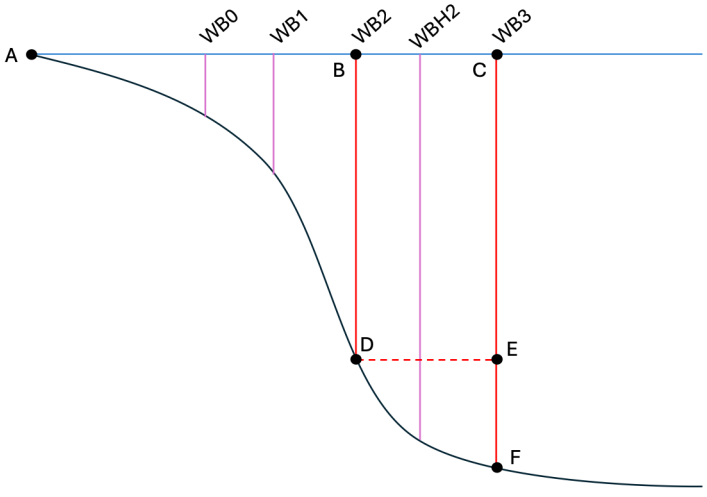


Figure A1. Schematic diagram of moorings on the western boundary. Red lines represent moorings WB2 (from the surface B to 3920 m D) and WB3 (from the surface C to 4840 m F), and magenta lines represent moorings WB0, WB1 and WBH2. In the previous methodology, the transport in D-E-F-D was only included in the streamfunction calculation when WB2 was unavailable. In the new methodology, the western boundary wedge transport is an estimate of the transport at each depth within the area bounded by A-B-D-A (above 3920m) and by D-E-F-D (below 3920m). The western dynamic height is then an estimate of the dynamic height on the concatenation of F-E and D-B. The reference level transport between D and E is estimated from current meter measurements and is used to calculate the barotropic transport within the area B-C-E-D-B. In the previous methodology this transport was not calculated and, therefore, was included in the compensation transport.

https://doi.org/10.5194/essd-2026-922
Preprint. Discussion started: 19 November 2026
© Author(s) 2026. CC BY 4.0 License.

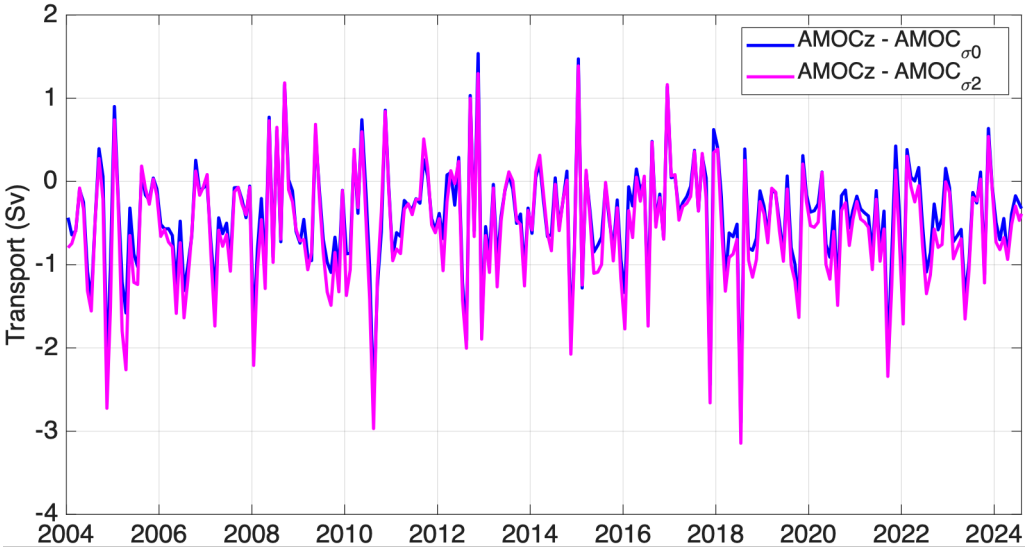


Figure A2. Difference between the AMOC timeseries evaluated in depth and density spaces, when the AMOC in density space is derived in (blue) σ_0-space and (magenta) σ_2-space.

Author contributions

TP produced the figures and prepared the original manuscript with contributions from all co-authors. BM, SE, RS and DV acquired funding. BM, SE, WJ, RS, DV, DS, TP, DR and JC contributed to the acquisition and processing of the RAPID measurements. BK completed the Argo analysis needed for the 2D method. WJ and EM developed the method for estimating property transports. DS developed the code for the 2D method, and AW completed the translation of the MATLAB code into PYTHON.

Competing interests

The contact author has declared that none of the authors has any competing interests.

Disclaimer

Copernicus Publications remains neutral with regard to jurisdictional claims made in the text, published maps, institutional affiliations, or any other geographical representation in this paper. While Copernicus Publications makes every effort to include appropriate place names, the final responsibility lies with the authors. Views expressed in the text are those of the authors and do not necessarily reflect the views of the publisher.

https://doi.org/10.5194/essd-2026-922
Preprint. Discussion started: 19 November 2026
© Author(s) 2026. CC BY 4.0 License.

Acknowledgements

We acknowledge and sincerely thank all those who have contributed to the acquisition, processing, quality control, and maintenance of the RAPID-MOCHA-WBTS observations over the past 20 years. This long-term observing programme would not have been possible without the sustained efforts of the scientists, engineers, technicians, ship crews, data managers, and other personnel involved in the development, maintenance and continuous improvement of the RAPID project.

Financial support

The RAPID AMOC observing project is supported by the UK Natural Environment Research Council Grants ATLANTiS (NE/Y005589/1) and RAPID Evolution (NE/Y003551/1), the US National Science Foundation (Grants 2148723 and 2334091), the NOAA's Global Ocean Monitoring and Observing program (Grant 100007298) and the NOAA Atlantic Oceanographic and Meteorological Laboratory.

References

Baringer, M. O., & Larsen, J. C. (2001). Sixteen years of Florida Current Transport at 27° N. *Geophysical Research Letters*, *28*(16), 3179–3182. https://doi.org/10.1029/2001GL013246

Berglund, S., Döös, K., Groeskamp, S., & McDougall, T. J. (2022). The downward spiralling nature of the North Atlantic Subtropical Gyre. *Nature Communications*, *13*(1), 1–9. https://doi.org/10.1038/s41467-022-29607-8

Biló, T. C., & Johns, W. E. (2020). The Deep Western Boundary Current and Adjacent Interior Circulation at 24°–30°N: Mean Structure and Mesoscale Variability. *Journal of Physical Oceanography*, *50*(9), 2735–2758. https://doi.org/10.1175/JPO-D-20-0094.1

Bryden, H. L., & Hall, M. M. (1980). Heat Transport by Currents Across 25°N Latitude in the Atlantic Ocean. *Science*, *207*(4433), 884–886. https://doi.org/10.1126/science.207.4433.884

Bryden, H. L., King, B. A., McCarthy, G. D., & McDonagh, E. L. (2014). Impact of a 30% reduction in Atlantic meridional overturning during 2009–2010. *Ocean Science*, *10*(4), 683–691. https://doi.org/10.5194/os-10-683-2014

Calafat, F. M., Vallivattathillam, P., & Frajka-Williams, E. (2025). Estimates of Atlantic meridional heat transport from spatiotemporal fusion of Argo, altimetry, and gravimetry data. *Ocean Science*, *21*(6), 2743–2762. https://doi.org/10.5194/os-21-2743-2025

Cunningham, S. A., Kanzow, T., Rayner, D., Baringer, M. O., Johns, W. E., Marotzke, J., Longworth, H. R., Grant, E. M., Hirschi, J. J.-M., Beal, L. M., Meinen, C. S., & Bryden, H. L. (2007). Temporal Variability of the Atlantic Meridional Overturning Circulation at 26.5°N. *Science*, *317*(5840), 935–938. https://doi.org/10.1126/science.1141304

https://doi.org/10.5194/essd-2026-922
Preprint. Discussion started: 19 November 2026
© Author(s) 2026. CC BY 4.0 License.

Cunningham, S. A., Roberts, C. D., Frajka-Williams, E., Johns, W. E., Hobbs, W., Palmer, M. D., Rayner, D., Smeed, D. A., & McCarthy, G. (2013). Atlantic Meridional Overturning Circulation slowdown cooled the subtropical ocean. *Geophysical Research Letters*, *40*(23), 6202–6207. https://doi.org/10.1002/2013GL058464

Foukal, N., Le Bras, I., Fu, Y., Petit, T., Biló, T., Elipot, S., & Moat, B. (2026). Strengthening Connections in Observing the North Atlantic Meridional Overturning Circulation: Outcomes from a Joint RAPID-OSNAP Workshop. *Oceanography*. https://doi.org/10.5670/oceanog.2026.e110

Fox, A. D., Fraser, N. J., Burmeister, K., Jones, S. C., Cunningham, S. A., Drysdale, L. A., Dilmahamod, A. F., & Karstensen, J. (2026). The Scotland–Canada overturning array (SCOTIA): twenty years of meridional overturning in the subpolar North Atlantic. *Ocean Science*, *22*(3), 1439–1456. https://doi.org/10.5194/os-22-1439-2026

Frajka-Williams, E., Cunningham, S. A., Bryden, H., & King, B. A. (2011). Variability of Antarctic Bottom Water at 24.5°N in the Atlantic. *Journal of Geophysical Research: Oceans*, *116*(C11). https://doi.org/10.1029/2011JC007168

Frajka-Williams, E., Foukal, N., & Danabasoglu, G. (2023). Should AMOC observations continue: How and why? In *Philosophical Transactions of the Royal Society A: Mathematical, Physical and Engineering Sciences* (Vol. 381, Number 2262). Royal Society Publishing. https://doi.org/10.1098/rsta.2022.0195

Fu, Y., Lozier, M. S., Bower, A., Burmeister, K., Carrilho Biló, T., Cyr, F., Cunningham, S. A., deYoung, B., Dilmahamod, A. F., de Jong, M. F., Fried, N., Holliday, N. P., Fraser, N. J., Johns, W. E., Li, F., Karstensen, J., Pickart, R. S., Straneo, F., & Yashayaev, I. (2025). Characterizing the Interannual Variability of North Atlantic Subpolar Overturning. *Geophysical Research Letters*, *52*(19). https://doi.org/10.1029/2025GL114672

Hersbach, H., Bell, B., Berrisford, P., Hirahara, S., Horányi, A., Muñoz-Sabater, J., Nicolas, J., Peubey, C., Radu, R., Schepers, D., Simmons, A., Soci, C., Abdalla, S., Abellan, X., Balsamo, G., Bechtold, P., Biavati, G., Bidlot, J., Bonavita, M., … Thépaut, J. (2020). The ERA5 global reanalysis. *Quarterly Journal of the Royal Meteorological Society*, *146*(730), 1999–2049. https://doi.org/10.1002/qj.3803

Jackson, L. C., Peterson, K. A., Roberts, C. D., & Wood, R. A. (2016). Recent slowing of Atlantic overturning circulation as a recovery from earlier strengthening. *Nature Geoscience*, *9*(7), 518–522. https://doi.org/10.1038/ngeo2715

Johns, W. E., Baringer, M. O., Beal, L. M., Cunningham, S. A., Kanzow, T., Bryden, H. L., Hirschi, J. J. M., Marotzke, J., Meinen, C. S., Shaw, B., & Curry, R. (2011). Continuous, Array-Based Estimates of Atlantic Ocean Heat Transport at 26.5°N. *Journal of Climate*, *24*(10), 2429–2449. https://doi.org/10.1175/2010JCLI3997.1

Johns, W. E., Beal, L. M., Baringer, M. O., Molina, J. R., Cunningham, S. A., Kanzow, T., & Rayner, D. (2008). Variability of Shallow and Deep Western Boundary Currents off the Bahamas during 2004–05: Results from the 26°N RAPID–MOC Array. *Journal of Physical Oceanography*, *38*(3), 605–623. https://doi.org/10.1175/2007JPO3791.1

Johns, W. E., Elipot, S., Smeed, D. A., Moat, B., King, B., Volkov, D. L., & Smith, R. H. (2023). Towards two decades of Atlantic Ocean mass and heat transports at 26.5° N. *Philosophical Transactions. Series A, Mathematical, Physical, and Engineering Sciences*, *381*(2262), 20220188. https://doi.org/10.1098/rsta.2022.0188

https://doi.org/10.5194/essd-2026-922
Preprint. Discussion started: 19 November 2026
© Author(s) 2026. CC BY 4.0 License.

Johns, W. E., Kanzow, T., & Zantopp, R. (2005). Estimating ocean transports with dynamic height moorings: An application in the Atlantic Deep Western Boundary Current at 26°N. *Deep Sea Research Part I: Oceanographic Research Papers*, *52*(8), 1542–1567. https://doi.org/10.1016/j.dsr.2005.02.002

Kanzow, T., Cunningham, S. A., Johns, W. E., Hirschi, J. J. M., Marotzke, J., Baringer, M. O., Meinen, C. S., Chidichimo, M. P., Atkinson, C., Beal, L. M., Bryden, H. L., & Collins, J. (2010). Seasonal variability of the Atlantic meridional overturning circulation at 26.5°N. *Journal of Climate*, *23*(21), 5678–5698. https://doi.org/10.1175/2010JCLI3389.1

Kanzow, T., Cunningham, S. A., Rayner, D., Hirschi, J. J.-M., Johns, W. E., Baringer, M. O., Bryden, H. L., Beal, L. M., Meinen, C. S., & Marotzke, J. (2007). Observed Flow Compensation Associated with the MOC at 26.5°N in the Atlantic. *Science*, *317*(5840), 938–941. https://doi.org/10.1126/science.1141293

Larsen, J. C. (1992). Transport and heat flux of the Florida Current at 27°N derived from cross-stream voltages and profiling data: theory and observations. *Philosophical Transactions of the Royal Society of London. Series A: Physical and Engineering Sciences*, *338*(1650), 169–236. https://doi.org/10.1098/rsta.1992.0007

McCarthy, G. D., Hug, G., Smeed, D., Morris, K. J., & Moat, B. (2025). Signal and Noise in the Atlantic Meridional Overturning Circulation at 26°N. *Geophysical Research Letters*, *52*(7). https://doi.org/10.1029/2025GL115055

McCarthy, G. D., Smeed, D. A., Johns, W. E., Frajka-Williams, E., Moat, B. I., Rayner, D., Baringer, M. O., Meinen, C. S., Collins, J., & Bryden, H. L. (2015). Measuring the Atlantic Meridional Overturning Circulation at 26°N. *Progress in Oceanography*, *130*, 91–111. https://doi.org/10.1016/j.pocean.2014.10.006

McCarthy, G., Frajka-Williams, E., Johns, W. E., Baringer, M. O., Meinen, C. S., Bryden, H. L., Rayner, D., Duchez, A., Roberts, C., & Cunningham, S. A. (2012). Observed interannual variability of the Atlantic meridional overturning circulation at 26.5°N. *Geophysical Research Letters*, *39*(19), 1–5. https://doi.org/10.1029/2012GL052933

McDonagh, E. L., King, B. A., Bryden, H. L., Courtois, P., Szuts, Z., Baringer, M., Cunningham, S. A., Atkinson, C., & McCarthy, G. (2015). Continuous Estimate of Atlantic Oceanic Freshwater Flux at 26.5°N. *Journal of Climate*, *28*(22), 8888–8906. https://doi.org/10.1175/JCLI-D-14-00519.1

Meinen, C. S., Baringer, M. O., & Garcia, R. F. (2010). Florida Current transport variability: An analysis of annual and longer-period signals. *Deep Sea Research Part I: Oceanographic Research Papers*, *57*(7), 835–846. https://doi.org/10.1016/j.dsr.2010.04.001

Meinen, C. S., Johns, W. E., Moat, B. I., Smith, R. H., Johns, E. M., Rayner, D., Frajka-Williams, E., Garcia, R. F., & Garzoli, S. L. (2019). Structure and Variability of the Antilles Current at 26.5°N. *Journal of Geophysical Research: Oceans*, *124*(6), 3700–3723. https://doi.org/10.1029/2018JC014836

Meinen, C. S., Speich, S., Piola, A. R., Ansorge, I., Campos, E., Kersalé, M., Terre, T., Chidichimo, M. P., Lamont, T., Sato, O. T., Perez, R. C., Valla, D., van den Berg, M., Le Hénaff, M., Dong, S., & Garzoli, S. L. (2018). Meridional Overturning Circulation Transport Variability at 34.5°S During 2009–2017: Baroclinic and Barotropic Flows and the Dueling Influence of the Boundaries. *Geophysical Research Letters*, *45*(9), 4180–4188. https://doi.org/10.1029/2018GL077408

https://doi.org/10.5194/essd-2026-922
Preprint. Discussion started: 19 November 2026
© Author(s) 2026. CC BY 4.0 License.



Moat B.I.; Petit T.; Smeed D.A.; Rayner D.; Johns W.E.; Smith, R.; Volkov, D.; Elipot S.; Baringer M. O.; and Collins, J. (2026). Atlantic meridional overturning circulation observed by the RAPID-MOCHA-WBTS (RAPID-Meridional Overturning Circulation and Heatflux Array-Western Boundary Time Series) array at 26N from 2004 to 2024 (v2024-2). NERC EDS British Oceanographic Data Centre NOC. doi:10.5285/5c39bf4e-5140-5546-e063-7086abc027bc

Petit, T., Smeed, D., Blaker, A., Elipot, S., Johns, W., Kajtar, J. B., Rayner, D., Sinha, B., Smith, R. H., Volkov, D. L., & Moat, B. (2025). Evaluation of a Reduced RAPID Array for Measuring the AMOC. *Journal of Geophysical Research: Oceans*, *130*(11). https://doi.org/10.1029/2025JC023093

Roemmich, D., & Wunsch, C. (1985). Two transatlantic sections: meridional circulation and heat flux in the subtropical North Atlantic Ocean. *Deep Sea Research Part A. Oceanographic Research Papers*, *32*(6), 619–664. https://doi.org/10.1016/0198-0149(85)90070-6

Smeed, D. A., Johns, W. E., Smith, R. H., Petit, T., McDonagh, E. L., Rayner, D., Volkov, D. L., Elipot, S., Kajtar, J. B., King, B. A., Firing, Y. L., & Moat, B. I. (2026). Overturning Circulation of the North Atlantic Subtropical Gyre Computed in Density Coordinates at 26°N. *Geophysical Research Letters*, *53*(5). https://doi.org/10.1029/2025GL118277

Smeed, D. A., Josey, S. A., Beaulieu, C., Johns, W. E., Moat, B. I., Frajka-Williams, E., Rayner, D., Meinen, C. S., Baringer, M. O., Bryden, H. L., & McCarthy, G. D. (2018). The North Atlantic Ocean Is in a State of Reduced Overturning. *Geophysical Research Letters*, *45*(3), 1527–1533. https://doi.org/10.1002/2017GL076350

Smeed, D. A., McCarthy, G. D., Cunningham, S. A., Frajka-Williams, E., Rayner, D., Johns, W. E., Meinen, C. S., Baringer, M. O., Moat, B. I., Duchez, A., & Bryden, H. L. (2014). Observed decline of the Atlantic meridional overturning circulation 2004–2012. *Ocean Science*, *10*(1), 29–38. https://doi.org/10.5194/os-10-29-2014

Srokosz, M., Baringer, M., Bryden, H., Cunningham, S., Delworth, T., Lozier, S., Marotzke, J., & Sutton, R. (2012). Past, Present, and Future Changes in the Atlantic Meridional Overturning Circulation. *Bulletin of the American Meteorological Society*, *93*(11), 1663–1676. https://doi.org/10.1175/BAMS-D-11-00151.1

Thomson, R. E., & Emery, W. J. (2014). *Data Analysis Method in Physical Oceanography* (Elsevier S).

Thresher, R. E., Rintoul, S. R., Fallon, S. J., Richer de Forges, S., Neil, H., Trotter, J. A., Proctor, C., & Tracey, D. M. (2026). Millennial-scale Atlantic overturning circulation led by the Southern Ocean. *Nature Geoscience*, *19*(5), 520–525. https://doi.org/10.1038/s41561-026-01959-6

Tooth, O. J., Foukal, N. P., Johns, W. E., Johnson, H. L., & Wilson, C. (2024). Lagrangian Decomposition of the Atlantic Ocean Heat Transport at 26.5°N. *Geophysical Research Letters*, *51*(14). https://doi.org/10.1029/2023GL107399

Trenberth, K. E., & Caron, J. M. (2001). Estimates of Meridional Atmosphere and Ocean Heat Transports. *Journal of Climate*, *14*(16), 3433–3443. https://doi.org/10.1175/1520-0442(2001)014<3433:EOMAAO>2.0.CO;2

Volkov, D. L., Perez, R. C., Atkinson, C. P., Beckley, B., Carter, B. R., Cetinić, I., Chan, D., Cheng, L., Domingues, C. M., Dong, S., Du, J., Elipot, S., Feely, R. A., Franz, B. A., Fu, Y., Gao, M., Garcia, H., Graham, G., Hamlington, B. D., … Zhou, Y. (2026). Global Oceans. *Bulletin of the American Meteorological Society*, *107*(8), S168–S234. https://doi.org/10.1175/BAMS-D-26-0100.1

https://doi.org/10.5194/essd-2026-922
Preprint. Discussion started: 19 November 2026
© Author(s) 2026. CC BY 4.0 License.



Volkov, D. L., Smith, R. H., & Garcia, R. F. (2025). Pressure Gauges and Satellite Altimetry Ensure the Continuity of Florida Current Transport Observations. *Geophysical Research Letters*, *52*(13). https://doi.org/10.1029/2025GL115897

Volkov, D. L., Smith, R. H., Garcia, R. F., Smeed, D. A., Moat, B. I., Johns, W. E., & Baringer, M. O. (2024). Florida Current transport observations reveal four decades of steady state. *Nature Communications*, *15*(1), 7780. https://doi.org/10.1038/s41467-024-51879-5

Wett, S., Rhein, M., Kieke, D., Mertens, C., & Moritz, M. (2023). Meridional Connectivity of a 25-Year Observational AMOC Record at 47°N. *Geophysical Research Letters*, *50*(16). https://doi.org/10.1029/2023GL103284

Winkelbauer, S., Forget, G., Mayer, M., Bourdalle-Badie, R., Cipollone, A., Haimberger, L., Haines, K., Osafune, S., Song, Y., Storto, A., Yang, C., & Zuo, H. (2026). Atlantic Meridional Heat Transports from Ocean Reanalyses, Monitored Sections and Heat Budget Constraints. *Ocean Science*. https://doi.org/10.5194/egusphere-2026-5435

Xing, Q., Elipot, S., Johns, W. E., Smeed, D. A., Moat, B. I., & Loder, J. W. (2026). Meridionally consistent decline in the observed western boundary contribution to the Atlantic Meridional Overturning Circulation. *Science Advances*, *12*(15). https://doi.org/10.1126/sciadv.adz7738

Yan, X., Zhang, R., & Knutson, T. R. (2018). Underestimated AMOC Variability and Implications for AMV and Predictability in CMIP Models. *Geophysical Research Letters*, *45*(9), 4319–4328. https://doi.org/10.1029/2018GL077378